Clinical Cancer Research

Preclinical Comparison of Osimertinib with Other EGFR-TKIs in EGFR-Mutant NSCLC Brain Metastases Models, and Early Evidence of Clinical Brain Metastases Activity

Peter Ballard[1], James W.T. Yates[2], Zhenfan Yang[3], Dong-Wan Kim[4], James Chih-Hsin Yang[5], Mireille Cantarini[6], Kathryn Pickup[1], Angela Jordan[1], Mike Hickey[7], Matthew Grist[1], Matthew Box[1], Peter Johnström[8,9], Katarina Varnäs[9], Jonas Malmquist[9], Kenneth S. Thress[10], Pasi A. Jänne[11], and Darren Cross[2]

Abstract

Purpose: Approximately one-third of patients with non–small cell lung cancer (NSCLC) harboring tumors with EGFR-tyrosine kinase inhibitor (TKI)-sensitizing mutations (EGFRm) experience disease progression during treatment due to brain metastases. Despite anecdotal reports of EGFR-TKIs providing benefit in some patients with EGFRm NSCLC brain metastases, there is a clinical need for novel EGFR-TKIs with improved efficacy against brain lesions.

Experimental Design: We performed preclinical assessments of brain penetration and activity of osimertinib (AZD9291), an oral, potent, irreversible EGFR-TKI selective for EGFRm and T790M resistance mutations, and other EGFR-TKIs in various animal models of EGFR-mutant NSCLC brain metastases. We also present case reports of previously treated patients with EGFRm-advanced NSCLC and brain metastases who received osimertinib in the phase I/II AURA study (NCT01802632).

Results: Osimertinib demonstrated greater penetration of the mouse blood–brain barrier than gefitinib, rociletinib (CO-1686), or afatinib, and at clinically relevant doses induced sustained tumor regression in an EGFRm PC9 mouse brain metastases model; rociletinib did not achieve tumor regression. Under positron emission tomography micro-dosing conditions, [^{11}C]osimertinib showed markedly greater exposure in the cynomolgus monkey brain than [^{11}C]rociletinib and [^{11}C]gefitinib. Early clinical evidence of osimertinib activity in previously treated patients with EGFRm-advanced NSCLC and brain metastases is also reported.

Conclusions: Osimertinib may represent a clinically significant treatment option for patients with EGFRm NSCLC and brain metastases. Further investigation of osimertinib in this patient population is ongoing. *Clin Cancer Res; 22(20); 5130–40.* *©2016 AACR.*

Introduction

A number of EGFR tyrosine kinase inhibitors (TKI) are recommended for first-line treatment of patients with advanced non–small cell lung cancer (NSCLC) harboring an EGFR-TKI–sensitizing mutation (EGFRm; refs. 1, 2). However, more than 30% of patients with NSCLC experience disease progression during treatment with established EGFR-TKIs due to growth of synchronous or metachronous brain metastases (3, 4).

For successful treatment of brain metastases, a drug must first be able to cross the blood–brain barrier (BBB). BBB penetration is influenced by factors such as a drug's affinity for the ATP-binding cassette efflux transporters, permeability glycoprotein (P-gp), and breast cancer-resistance protein (BCRP), which are involved in the removal of toxins, drugs, and chemotherapies from the central nervous system (CNS; refs. 5–9). Chemotherapy agents and large monoclonal antibodies are generally unable to cross the BBB (7, 10). The ability of a molecule to cross the BBB is affected by multiple factors, including molecular weight (11).

Active or untreated brain metastases are often exclusion criteria in trials of EGFR-TKIs; however, there are reports documenting efficacy of EGFR-TKIs in treatment of, and/or preventing development of, brain metastases in patients with EGFRm NSCLC (12–15). In a retrospective analysis of 155 patients, initial gefitinib or erlotinib treatment was associated with a lower cumulative risk of CNS progression (1%, 6%, and 21% at 6, 12, and 24 months) compared with chemotherapy (7%, 19%, and 32%, respectively; ref. 12). In addition, pulsatile

[1]iMED Oncology, AstraZeneca, Macclesfield, United Kingdom. [2]iMED Oncology, AstraZeneca, Cambridge, United Kingdom. [3]Asia and Emerging Markets iMED, AstraZeneca, Shanghai, China. [4]Department of Internal Medicine, Seoul National University Hospital, Seoul, Korea. [5]National Taiwan University Hospital, Taipei City, Taiwan. [6]Global Medicines Development, AstraZeneca, Macclesfield, United Kingdom. [7]AstraZeneca, Cambridge, United Kingdom. [8]AstraZeneca Translational Science Centre, Stockholm, Sweden. [9]Department of Clinical Neuroscience, Karolinska Institutet, Stockholm, Sweden. [10]iMED Oncology, AstraZeneca, Gatehouse Park, Waltham, Massachusetts. [11]Dana-Farber Cancer Institute, Boston, Massachusetts.

Note: Supplementary data for this article are available at Clinical Cancer Research Online (http://clincancerres.aacrjournals.org/).

Corresponding Authors: Darren Cross, iMed Oncology, AstraZeneca, Cambridge, United Kingdom. Phone: 447876 875414; E-mail: Darren.Cross@astrazeneca.com; and Peter Ballard, pbdmpk@gmail.com

doi: 10.1158/1078-0432.CCR-16-0399

Translational Relevance

There is a clinical need for novel EGFR-tyrosine kinase inhibitors (EGFR-TKI) with improved efficacy against brain lesions. Disease progression due to brain metastases is common in patients with non–small cell lung cancer (NSCLC) harboring tumors with EGFR-TKI–sensitizing mutations (EGFRm). As such, the exposure and activity in the brain of osimertinib was analyzed. We present data that indicate that osimertinib had greater exposure in the brain compared with some other EGFR-TKIs (gefitinib, afatinib, and rociletinib), and demonstrated activity against EGFRm NSCLC brain metastases in preclinical models and early clinical reports. Osimertinib has potential as a pharmacologic treatment for patients with EGFRm NSCLC and brain metastases and may provide an important step forward, given the limitations experienced with existing treatment options.

administration of high-dose erlotinib can control CNS metastases from EGFR-mutant NSCLC (16).

Despite reports of tumor responses, the TKIs gefitinib, erlotinib, and afatinib are considered to have generally poor biopharmaceutical properties for penetrating the BBB, perhaps attributable to interactions with P-gp and BCRP (17–19). However, penetration may be increased in patients with more advanced brain metastases where BBB disruption has already occurred (20–22). In addition, there is a cumulative increase in brain metastases incidence in patients with EGFRm NSCLC over time (23). Although many patients die of systemic progression, rather than brain lesion progression, quality of life is significantly worsened, both directly and as a result of whole brain radiotherapy (WBRT), which degrades cognitive function (24). In addition, as systemic therapies improve for patients with EGFRm NSCLC, the brain may increasingly become a sanctuary site where the BBB may offer protection from pharmacological agents (22). Therefore, there exists a clinical need for EGFR-TKIs with improved BBB penetration, and it is important that new mutant-selective agents, such as osimertinib (AZD9291), an oral, potent, irreversible EGFR-TKI selective for sensitizing and T790M-resistance mutations (25, 26), and rociletinib (CO-1686; ref. 27), are explored in this context.

Osimertinib was recently approved by the FDA for treatment of patients with NSCLC harboring a T790M mutation, and whose disease has progressed following treatment with another EGFR-TKI (28). We examined the brain exposure and distribution of osimertinib and the active metabolites AZ5104 and AZ7550 in the preclinical setting. We compared brain distribution, pharmacokinetics (PK), and *in vivo* brain xenograft efficacy of osimertinib with other EGFR-TKIs and simulated potential clinical efficacy based on these data. Furthermore, brain penetration of radiolabeled osimertinib and other EGFR-TKIs was examined in a nonhuman primate model. We also present early evidence of clinical efficacy of osimertinib against brain metastases as part of the ongoing AURA trial (NCT01802632).

Materials and Methods

Test compounds and cell lines

Madin-Darby canine kidney (MDCK) epithelial cells were obtained from U.S. National Institutes of Health, Bethesda, MD, and Netherlands Cancer Institute [multidrug-resistance protein 1 (MDR1)-MDCK]; Absorption Systems and AstraZeneca (BCRP-MDCK); ATCC (Caco2). Cells were authenticated during each experiment by monitoring transepithelial electrical resistance, and with positive controls. H1975 cells were obtained from ATCC in 2004, and authenticated by short-tandem repeat analysis in November 2012. PC9 cells (exon 19 deletion) were obtained in November 2011 from Akiko Hiraide at Preclinical Sciences R&D, AstraZeneca, and tested and authenticated by short-tandem repeat analysis in May 2013.

Details on cell line maintenance and test compounds are presented as Supplementary Information.

Permeability glycoprotein and breast cancer resistance protein substrate assessment

P-gp (also known as MDR1) and BCRP substrate assessments of osimertinib, AZ7550, AZ5104, rociletinib, afatinib, and erlotinib were performed using transfected MDCK cells (MDR1-MDCK; BCRP-MDCK) and the Caco2 (colon carcinoma) cell line. Digoxin, cladribine, and Ko143 10 mmol/L, valspodar 1 mmol/L, and atorvastatin 0.075 mmol/L stock solutions in DMSO were prepared as positive controls or inhibitors.

Cell monolayers were grown onto collagen-coated, 12-well, polycarbonate membranes in Costar Transwell plates (1.13 cm^2 insert area, 0.4 μm pore size; Corning Life Sciences). Test and control compound substrate assessments were carried out in triplicate in each direction (apical [AP]-to-basolateral [BL], and BL-to-AP), co-dosed with 200 μmol/L Lucifer yellow (LY). Aliquots were taken from the test compound receiver compartment at preselected time points and replaced with an equal volume of fresh transport buffer. Positive control receiver samples were taken at 120 minutes. LC/MS-MS was used for analysis of the test compound, and LY concentration measured using a BMG microplate reader (excitation 485 nm; emission 540 nm). Donor sample aliquots were taken at selected time points without replacement.

Relative efflux ratios of compounds between MDR1-MDCK or BCRP-MDCK cells, compared with nontransfected MDCK cells, and co-dosing with 1 μmol/L valspodar or 10 μmol/L Ko143, were utilized to verify whether test compounds were P-gp and BCRP substrates, respectively.

For Caco2 drug transport assays, atenolol (low permeability marker), minoxidil (high permeability marker), and digoxin (control efflux marker) were prepared in DMSO to a test concentration of 10 μmol/L. To determine test and control compound transport rates in AP-to-BL and BL-to-AP directions, LY 100 μmol/L was run alongside all compounds. Donor samples were taken at 60 and 120 minutes, and receiver samples taken additionally at 30 and 60 minutes and replaced with an equal volume of fresh transport buffer.

Apparent permeability coefficients of test compounds across Caco2 monolayers was estimated using high-performance liquid chromatography (HPLC)/MS-MS; LY concentrations were measured using an Infinite 200 PRO microplate reader (485 nmol/L excitation; 530 nmol/L emission).

Rat quantitative whole body autoradiography

Tissue distribution of radioactivity in male partially pigmented (Lister-Hooded) rats was determined following a single oral dose of [^{14}C]osimertinib (4 mg/kg, 7.4 MBq/kg) as a suspension in aqueous hydroxypropyl methylcellulose

[HPMC; 0.5% (w/v)]. Rats were terminated under anesthesia by cold shock at 0.5, 1, 6, and 24 hours, and 2, 7, 21, and 60 days post-dose. Animals were immersed in a freezing mixture for ≥30 minutes and subjected to sagittal plane whole body sectioning (nominal thickness 30 μm). Concentration of radioactivity in tissues was determined using quantitative whole body autoradiography (QWBA) by Covance Laboratories Ltd. using a validated image analysis system.

In a separate experiment, the distribution of a single oral dose of [^{14}C]gefitinib (5 mg/kg, 8.3 MBq/kg) in male Pievald Virol Glaxo pigmented rats was assessed. [^{14}C]gefitinib was administered as a suspension in 0.5% HPMC in 0.1% polysorbate 80. Rats were terminated by CO_2 narcosis at 1, 2, 6, 24, 48, and 96 hours postdose and frozen and sectioned as above. Radioactivity was quantified using a Phosphor Imager SF (Molecular Dynamics).

Brain binding *in vitro*

Brain tissue from treatment-naïve nude mice was homogenized with PBS (1:3, w/w), and [^{3}H]osimertinib spiked into the blank brain homogenate at a 5 μmol/L final concentration. Radioactive content of spiked brain homogenate was assessed by liquid scintillation counting (LSC) using Ultima Gold Scintillation cocktail. Samples were counted for 10 minutes, or until 10^5 counts had accumulated; test compound concentrations were calculated using the radioactive content of each sample in conjunction with the specific activity of the material used. Spiked brain homogenate was dialyzed in triplicate against PBS for 4 hours at 37°C using Spectra/Por2 equilibrium dialysis membrane discs (molecular weight cut-off of 12–14 kDa; Spectrum Laboratories Inc.). Aliquots of brain homogenate and PBS were assessed by LSC; the free fraction of test compounds in brain homogenate was calculated and overall recovery of radioactivity from cells determined. The free fraction in undiluted brain was determined from these data.

The *in vitro* brain binding assays of unlabeled osimertinib was carried out on a HT-Dialysis plate (HTD 96 b, Cat. no. 1006). Blank brain homogenate (1:3 with Dulbecco's PBS pH 7.4) was spiked with 5 μmol/L test compound (in triplicate) and dialyzed (molecular weight cut-off 12–14 kDa) against 100 mmol/L PBS buffer (pH 7.4), slowly rotated at 37°C for 4 hours. Receiver and donor aliquots were taken following incubation, and donor samples further diluted. Paired samples were matrix-matched with buffer or blank brain homogenate, and precipitated with cold acetonitrile with internal standard. After centrifuging at 4000 rpm for 20 minutes, supernatant was diluted with 0.1% formic acid aqueous solution and analyzed by LC-MS/MS (API 4000; Applied Biosystems).

The *in vitro* brain binding assay of unlabeled gefitinib was carried out on a RED device system (Thermo Fisher Scientific) with a semipermeable membrane. Gefitinib 10 mmol/L was prepared in DMSO, and a 1 mmol/L working solution spiked in triplicate into blank brain homogenate (1:3 with PBS pH 7.4) to a 5 μmol/L final concentration; the final percentage volume of the organic solvent was 0.5%. Spiked brain homogenate was dialyzed against PBS pH 7.4 for 4 hours at 37°C with 5% CO_2 for 4 hours on a slowly rotating orbital shaker. Following incubation, a 50 μL receiver aliquot, and a 5 μL donor aliquot were taken; the donor sample was diluted with 45 μL of blank brain homogenate. Paired samples were matrix-matched with buffer or blank brain homogenate, mixed for 2 minutes, and precipitated with 150 μL cold acetonitrile containing internal standard. Samples were centrifuged at 4,000 × *g* for 20 minutes and supernatant diluted 1:2 with distilled water for LC/MS-MS (Waters Xevo TQ).

Mouse PK studies

Osimertinib was administered orally to female CB17 SCID mice bearing H1975 tumor xenografts at Oncodesign Biotechnology. Three mice per dose group and time point received osimertinib 5 or 25 mg/kg (as suspension in 0.5% HPMC). Mice were terminated (isoflurane overdose) and blood, brain, and tumor samples collected at 0.5, 1, 2, 4, 6, and 24 hours postdose.

Osimertinib 25 mg/kg, gefitinib 6.25 mg/kg, rociletinib 100 mg/kg, or afatinib 7.5 mg/kg were dosed to naïve female nude mice, with animals terminated (rising CO_2 dose) and blood and brain samples collected at 1, 2, and 6 hours postdose.

Plasma was prepared from blood in lithium heparin chilled tubes immediately after collection. Test compounds were extracted by protein precipitation using acetonitrile, containing internal standard (AZ10024306) in a 4:1 solvent:sample ratio. Samples were centrifuged for 10 minutes at 3,000 rpm; 50 μL of supernatant was combined with 300 μL of water before HPLC/MS-MS.

Brain and tumor samples were cut into two portions prior to snap freezing in liquid nitrogen, stored at −80°C, and transferred to Oncology DMPK, AstraZeneca R&D. Following thawing, samples were transferred to FastPrep Lysing Matrix A tubes (MP Biomedicals LLC). Water was added (1:3 tissue:water w/v) and samples homogenized; homogenate was treated in the same way as plasma.

Exposure was expressed as area under the plasma or tissue–concentration time curve (AUC) from 0 to 6 or 0 to 24 hours according to the last concentration measured. Maximum observed concentration (C_{max}) and time to C_{max} (t_{max}) were direct observations of concentration versus time data. PK parameters were obtained by means of noncompartmental analysis using Phoenix32 version 6.4 (Pharsight Corporation).

Cynomolgus monkey PET micro-dosing

A PET microdosing study was performed in four cynomolgus monkeys (Supplementary Table S2). Monkeys were anesthetized using ketamine, and anesthesia maintained by a mixture of O_2, air, and sevoflurane (2–8%). Anesthesia, heart rate, blood pressure, and body temperature were continuously monitored. Radiolabeled compounds were injected as a bolus into a sural vein. Injected radioactivity was 141 ± 25 MBq corresponding to <3 μg of radiolabeled osimertinib, AZ5104, gefitinib, and rociletinib. The distribution of radioactivity following intravenous microdosing was assessed using PET imaging more than 125 minutes with a Siemens molecular imaging high-resolution research tomograph system (29). Arterial blood samples were collected and analyzed for radioactivity in blood. Separate experiments were conducted to determine radioactivity distribution to the brain and abdomen. Radioactivity concentration in brain was calculated and normalized to arterial blood radioactivity concentration as described in the Supplementary Material.

Mouse brain metastases xenograft

Effects of chronic once daily (QD) dosing of osimertinib, gefitinib, and rociletinib were assessed in a mouse brain metastases model. The human NSCLC cell line PC9 (exon 19 deletion) was transfected with the GL4.50[luc2/CMV/Hygro] vector

containing the luciferase gene (PC9_Luc) using lipofectamine LTX in order to monitor brain tumor growth by measuring bioluminescence signals in tumor cells (30, 31). Signal intensity was measured using the Bright-Glo Luciferase Assay System (Promega). The *EGFR* exon 19 deletion mutation was further confirmed in the PC9_Luc cell line.

For the brain metastases model, PC9_Luc cells were implanted into 6- to 8-week-old specific-pathogen-free immunodeficient nude mice purchased from Vital River by intra-internal carotid artery injection (32, 33). Bioluminescence signals were measured with an IVIS Xenogen imaging system weekly to monitor tumor growth. When signals reached the range of 10^7 photons/second, mice were randomized to be treated orally with osimertinib 5 or 25 mg/kg QD, gefitinib 6.25 mg/kg QD, rociletinib 100 mg/kg QD, or vehicle for 8 weeks. Bioluminescence signals (antitumor efficacy) and body weight (tolerability) were measured weekly; tumor growth inhibition was assessed by comparing mean bioluminescence intensity change for control and treated groups.

Pharmacokinetic–pharmacodynamic modeling

A series of modeling studies was undertaken to predict active doses of osimertinib in humans by incorporating human PK data into a previously developed PK-pharmacodynamic (PKPD) PC9 subcutaneous xenograft efficacy model that linked phosphorylated EGFR (pEGFR) inhibition to reductions in tumor volume (34). The studies also accounted for reduced free concentrations in the brain due to higher levels of binding than observed in plasma.

The PD model represents pEGFR, relative to control, as a pool homogenously distributed across the cell and cells in the tumor. The reversible interaction (docking) of the molecule with the receptor is assumed to be more rapid than the covalent binding step and subsequent deactivation of the receptor. The system is simplified with the reversible interaction characterized by the binding affinity, and the irreversible interaction characterized by a binding constant for unbound parent and metabolite. Further information on the model is presented as supplementary material.

Clinical case studies

We present two clinical case studies from the dose escalation/expansion component of the ongoing phase I/II AURA study (ClinicalTrials.gov: NCT01802632; ref. 35). In these cases, presence of brain metastases was documented at study entry; patients underwent magnetic resonance imaging of the brain at baseline and every 6 weeks thereafter as part of the systemic evaluation of disease status according to RECIST version 1.1 until disease progression.

Results

Osimertinib is a substrate of P-gp and BCRP transporters

Two efflux transporters, P-gp and BCRP, prevent molecules from crossing the BBB, so it was important to determine the level of osimertinib substrate activity against these transporters. Assessments were carried out in transwell plates in AP-to-BL and BL-to-AP directions (Fig. 1). Relative efflux ratios of osimertinib or its metabolite AZ5104 between MDR1-MDCK and normal MDCK cells and between BCRP-MDCK and MDCK cells suggest that these agents are P-gp and BCRP transporter substrates. When dosed in the presence of transporter inhibitors valspodar or Ko143, efflux ratios were similar to that observed in nontransfected MDCK or BCRP-MDCK cells, respectively. Collectively, data confirm that osimertinib and AZ5104 are substrates of P-gp and BCRP. The apparent permeability of AZ7550 in the BL-to-AP direction of MDR1-MDCK cells in the presence of valspodar or BCRP-MDCK cells in the presence of Ko143 suggests that AZ7550 is also a substrate of P-gp and BCRP.

In MDCK-MDR1 cells, efflux ratios of test compounds dosed at 1 μmol/L were 13.4 for osimertinib, 5.38 for rociletinib, 4.62 for afatinib, and 4.63 for erlotinib. Efflux ratios in MDCK-BCRP cells were 5.4 for osimertinib, 54.6 for afatinib, and 6.39 for erlotinib.

Osimertinib demonstrated a passive permeability profile across Caco2 cell monolayers, with no concentration dependence when tested at 1, 10, and 50 μmol/L, and an efflux ratio <2.0. The high-binding propensity of osimertinib to cells and plasticware led to low recovery values in this *in vitro* study (data not shown). The present osimertinib data indicate an efflux ratio of 0.372 for osimertinib 50 μmol/L (Supplementary Table S1). In this cell line, the efflux ratios were 4.61 for rociletinib 10 μmol/L and 11.5 for afatinib 10 μmol/L.

Rat quantitative whole body autoradiography indicates that osimertinib achieves brain exposure

To begin to directly explore the extent that osimertinib can achieve brain exposure following oral dosing (4 mg/kg), we utilized QWBA in rat with radiolabeled osimertinib. The tissue exposure pattern in male pigmented animals indicated that radioactivity associated with [^{14}C]osimertinib was rapidly absorbed and distributed into the brain, suggesting that drug-related radioactivity may have crossed the BBB. Maximum concentrations of total radioactivity were recorded in the blood and various tissues, including the brain at 6 hours postdose; the concentration of total radioactivity in blood and brain was 0.552 and 1.02 nmol equivalents/g, respectively. The maximum brain:blood ratio was approximately 2.2, achieved by 60 minutes postdose (Supplementary Fig. S2). Distribution was maintained in the brain up to 21 days after a single dose, although the brain:blood ratio (0.2) had decreased, and was below the lower limit of quantification in blood and brain at 60 days.

In comparison, gefitinib achieved little brain exposure following oral dosing (5 mg/kg), with 0.36 nmol equivalents/g detected in brain and a brain:blood ratio of approximately 0.69, achieved by 6 hours postdose. Gefitinib levels in the brain were below the limit of quantification by 24 hours postdose.

Osimertinib exhibits high brain binding *in vitro* and high distribution to mouse brain

Osimertinib was highly bound in mouse brain tissue *in vitro*. Dilution-corrected fractions of unbound osimertinib and [^{3}H]osimertinib in brain homogenate were 0.0009 and 0.0012 (standard error for both = 0.0002), with no statistically significant difference between datasets (P = 0.3059). The fraction of unbound gefitinib was 0.0052 (SE = 0.0002).

Although protein binding and efflux activity are important parameters contributing to BBB penetrance, they may not predict overall brain distribution. The rat QWBA study indicated that osimertinib-related material could penetrate the brain, so we were interested to discover if this radioactivity

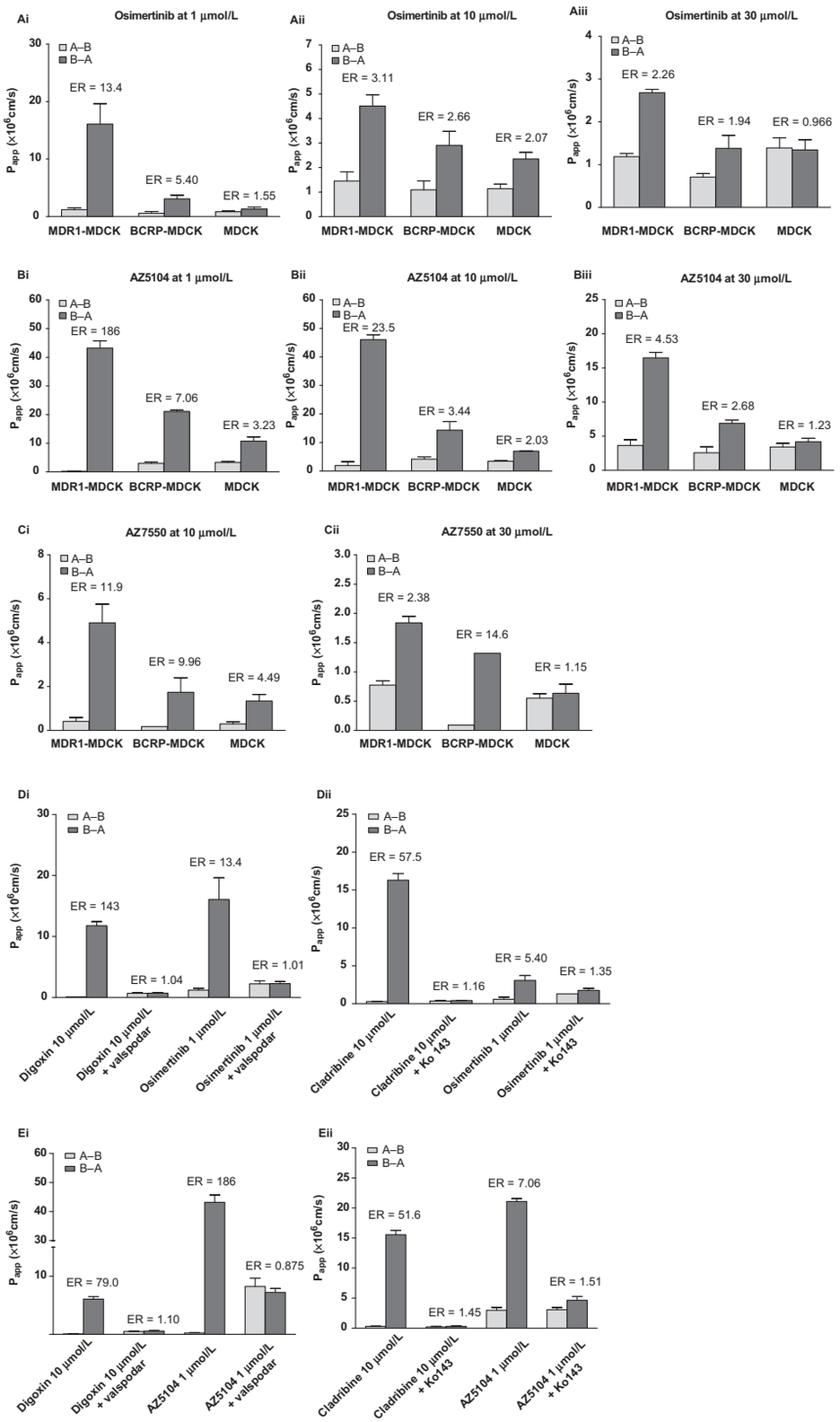

Figure 1.

Permeability of (**A**) osimertinib (**i,** 1 μmol/L; **ii,** 10 μmol/L; **iii,** 30 μmol/L), (**B**) AZ5104 (**i,** 1 μmol/L; **ii,** 10 μmol/L; **iii,** 30 μmol/L), and (**C**) AZ7550 (**ii,** 10 μmol/L; **ii,** 30 μmol/L) across MDR1-MDCK, BCRP-MDCK, and MDCK cell monolayers; (**D, i**.) digoxin (10 μmol/L) and osimertinib (1 μmol/L) in the presence or absence of valspodar across MDR1–MDCK cell monolayers; (**D, ii**) cladribine (10 μmol/L) and osimertinib (1 μmol/L) in the presence or absence of Ko143 across BCRP–MDCK cell monolayers; (**E, i**) digoxin (10 μmol/L) and AZ5104 (1 μmol/L) in the presence or absence of valspodar across MDR1–MDCK cell monolayers; (**E, ii**) cladribine (10 μmol/L) and AZ5104 (1 μmol/L) in the presence or absence of Ko143 across MDR1–MDCK cell monolayers. All data presented as mean ± SD. For positive controls, >99% inhibition of digoxin efflux in MDR1–MDCK and cladribine efflux in BCRP–MDCK cells was observed, indicating that P-gp and BCRP functioned normally in the test systems. **A,** apical side; **B,** basolateral side; BCRP, breast cancer resistance protein; ER, efflux ratio; MDCK, Madin-Darby canine kidney epithelial; MDR1, multidrug resistance protein 1; P-gp, permeability glycoprotein.

could be attributed to osimertinib and/or its metabolites. As a consequence, we measured osimertinib brain distribution directly *in vivo* in mouse following oral dosing at 5 and 25 mg/kg. Osimertinib was highly distributed in brain, to a similar extent as in tumor, resulting in AUC tissue:plasma ratios of 1.7 to 2.8 (Table 1). Furthermore, osimertinib was more

Table 1. Osimertinib, AZ5104, and AZ7550 pharmacokinetics in plasma, brain, and H1975 tumor following oral administration of osimertinib at 5 and 25 mg/kg to female SCID mice

	Dose (mg/kg)	5			25		
Test compound	**Tissue**	**Plasma**	**Brain**	**Tumor**	**Plasma**	**Brain**	**Tumor**
Osimertinib	C_{max} (μmol/L)	1.92	1.03	0.69	2.98	7.13	5.79
	t_{max} (hours)	0.5	2	4	0.5	4	4
	AUC_{0-t} (μmol/L.h/L)	4.82	8.56	8.19	23.9	67.0	66.2
	$t_{1/2}$ (hours)	2.85	3.09	5.90	2.81	3.48	6.68
	Tissue/plasma AUC ratio	NA	1.8	1.7	NA	2.8	2.8
AZ5104	C_{max} (μmol/L)	0.21	0	0.07	0.86	0	0.66
	t_{max} (h)	2	0	6	4	0	6
	AUC_{0-t} (μmol/L.h/L)	1.02	0	0.26	10.5	0	9.03
	Tissue/plasma AUC ratio	NA	ND	0.26	NA	ND	0.86
AZ7550	C_{max} (μmol/L)	0.27	0	0.15	0.64	0.16	1.08
	t_{max} (hours)	0.5	0	4	4	4	4
	AUC_{0-t} (μmol/L.h/L)	1.14	0	0.72	8.07	0.80	15.8
	Tissue/plasma AUC ratio	NA	ND	0.63	NA	0.10	2.0

Abbreviations: AUC, area under the plasma or tissue concentration–time curve; AUC_{0-t}, area under the plasma or tissue concentration–time curve from time 0 to time t; C_{max}, maximum plasma concentration; NA, not applicable; ND, not determined; $t_{1/2}$, terminal half-life; t_{max}, time to C_{max}.

highly distributed to mouse brain than gefitinib, rociletinib, or afatinib (Table 2). The brain:plasma C_{max} ratio for osimertinib was 3.41. In comparison, ratios for gefitinib, rociletinib, and afatinib were only 0.21, <0.08, and <0.36, respectively, with brain concentrations of rociletinib and afatinib below the assay lower limit of quantification. The unbound brain-to-plasma partition ratio ($Kp_{uu,brain}$) was 0.39 and 0.02, for osimertinib and gefitinib, respectively, but could not be determined for rociletinib and afatinib.

Of interest, based on AUC from time 0 to time t (AUC_{0-t}), the osimertinib metabolites AZ5104 and AZ7550 were observed at 21% to 44% and 24% to 34% of osimertinib at 5 and 25 mg/kg, respectively. AZ5104 exposure in tumor was at somewhat lower levels than observed in plasma; tumor:plasma ratios ranged from 0.26 to 0.86 (Table 1). However, in contrast to parent, no AZ5104 concentrations above the assay limit of detection (0.08 μmol/L) were measurable in brain (Table 1). Similarly, AZ7550 exposure in tumor was at similar levels to that observed in plasma; tumor:plasma ratios ranged from 0.63 to 2.0 (Table 1). AZ7550 showed minimal brain distribution with a brain:plasma ratio of 0.1 determined at the 25 mg/kg dose; distribution in brain was below the assay lower limit of detection (0.02 μmol/L) at 5 mg/kg (Table 1).

Osimertinib displays brain exposure in a cynomolgus monkey PET microdosing model

To further investigate osimertinib brain exposure using a quantitative imaging of radiolabeled drug approach, we used PET microdosing in cynomolgus monkeys. Under microdosing conditions (total dose <3 μg), [^{11}C]osimertinib showed marked exposure in the cynomolgus monkey brain in contrast to its active metabolite [^{11}C]AZ5104, and other EGFR-TKIs (Fig. 2). Following intravenous administration of [^{11}C]osimertinib, distribution to the brain was fast, plateauing at 1.29% ± 0.42% (N = 3) of injected radioactivity within 10 minutes. In contrast, administration of [^{11}C]AZ5104 (0.17%; N = 2), [^{11}C]gefitinib (0.11%; N = 2), and [^{11}C]rociletinib (0.023%; N = 2) resulted in very low brain exposure, with no regional differences in brain radioactivity observed. Ratios of the area under the brain radioactivity concentration–time curve from 0 to 90 minutes to that for blood radioactivity were calculated for [^{11}C]osimertinib (2.62 ± 1.42), [^{11}C]AZ5104 (0.35), [^{11}C]gefitinib (0.28), and [^{11}C]rociletinib (0.025).

Assessment of whole body distribution up to 120 minutes postdose revealed extensive hepatobiliary excretion of [^{11}C]rociletinib; hepatobiliary excretion of [^{11}C]osimertinib and [^{11}C]gefitinib occurred to a lower degree at a slower rate (Fig. 2).

No adverse effects or significant changes in physiological or blood parameters related to administration of radioactive test compounds were observed.

Table 2. Distribution to mouse brain of osimertinib, gefitinib, rociletinib, and afatinib following oral administration

	Osimertinib	Gefitinib	Rociletinib	Afatinib
Dose (mg/kg)	25	6.25	100	7.5
Plasma C_{max} (μmol/L)	0.82	0.82	3.32	0.14
Brain C_{max} (μmol/L)	2.78	0.17	BLQ	BLQ
Brain/plasma C_{max} ratio	3.41	0.21	<0.08	<0.36

NOTE: Doses equivalent to clinical doses or reported previously.
Abbreviation: BLQ, below limit of quantification (rociletinib 0.25 μmol/L, afatinib 0.05 μmol/L); C_{max}, maximum plasma concentration.

Osimertinib causes regression in a mouse EGFRm brain metastases model

As the PK and PET studies supported brain penetration of osimertinib, but not its metabolites, we explored how this translated into antitumor activity in a mouse PC9 (exon 19 deletion) xenograft brain metastases model. For this aggressively growing tumor model, there was only one control animal from a cohort of six still on study after day 50, as the tumor in this mouse grew slower than in other controls. Consequently, the control growth curve is observed to decrease after day 50 (Fig. 3A). A dose-dependent tumor regression was achieved with osimertinib (Fig. 3A), which correlated with overall survival (Fig. 3B). The dose of osimertinib 25 mg/kg QD, roughly equating to the 80 mg QD clinical dose of osimertinib in terms of exposure, was well tolerated and induced sustained tumor regression until study end at day 60, with a little weight loss at the initial time point and no subsequent decrease throughout the dosing period (Fig. 3C). Although the lower 5 mg/kg QD dose of osimertinib also caused tumor regression, it was more transient, only occurring in the first 3 weeks (Fig. 3A). In contrast, no tumor regression was achieved with rociletinib 100 mg/kg, approximately equivalent to a 500 mg twice daily human dose, and no survival benefit was observed (Fig. 3). A clinically relevant dose of gefitinib

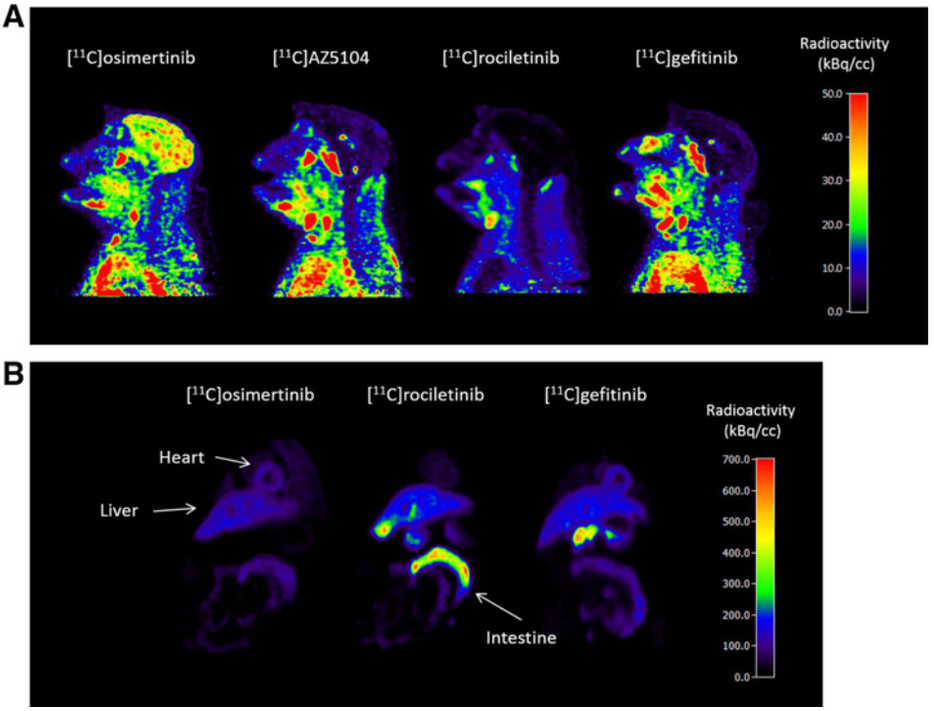

Figure 2.
PET images following administration of microdoses of [^{11}C]osimertinib, [^{11}C]AZ5104, [^{11}C]rociletinib, and [^{11}C]gefitinib to cynomolgus monkeys. **A,** color-coded PET images showing distribution of radioactivity in the brain of monkey ID#0702004 (average data from 5 to 123 minutes are shown); **B,** color-coded PET images showing distribution in the hepatobiliary system of radioactivity for [^{11}C]osimertinib and [^{11}C]rociletinib (monkey ID #0610010), and [^{11}C]gefitinib (monkey ID #0702004; average data from 0 to 123 minutes are shown; data for AZ5104 unavailable).

6.25 mg/kg, approximating to the exposure of a 250 mg QD human clinical dose, also demonstrated only transient tumor regression, for up to 20 days (Supplementary Fig. S3).

Predicting osimertinib clinical brain metastasis activity using PK-PD modeling

Overall, preclinical data indicated that osimertinib could potentially achieve efficacy in mutant EGFRm brain metastases. We therefore wanted to translate this into a clinical context using a PKPD modeling approach. The plasma PKPD model for osimertinib was adjusted according to mouse BBB penetration and binding data. After adjusting for control growth, simulated efficacy suggested that the model adequately predicted efficacy (Fig. 4), validating the assumption of adjusting for free exposure in the brain metastases model. Simulation based on subcutaneous xenograft models and free brain exposure to osimertinib revealed that higher doses were needed to achieve the same percentage tumor growth inhibition of brain metastases as seen in the primary tumor (Fig. 4), potentially due to lower free exposure of osimertinib and AZ5104 in the brain than systemically. Tumor growth simulations using human exposure of osimertinib predicted that a human dose of at least osimertinib 80 mg QD could be sufficient to target EGFRm NSCLC brain metastases.

Proof of principle clinical brain metastases activity of osimertinib in clinical case studies

As clinical proof of principle to support the preclinical findings, we report two clinical case studies (Fig. 5.) demonstrating evidence of clinical activity of osimertinib in brain metastases observed in the AURA phase I/II study (NCT01802632) in patients with acquired resistance to current EGFR-TKIs (35).

Case study 1 is of a 62-year-old Asian female diagnosed with EGFRm (exon 19 deletion) advanced NSCLC. This patient had been previously treated with gemcitabine/cisplatin for four cycles [outcome: stable disease (SD)], gefitinib between June 2011 and October 2012 [partial response (PR)], and pemetrexed for 10 cycles between November 2012 and June 2013 (SD), with WBRT between December 2012 and January 2013. Biopsy in July 2013 identified T790M mutation. The patient started osimertinib 40 mg QD in a T790M positive expansion cohort of the AURA clinical study on August 7, 2013. PR was achieved from the 12-week Response Evaluation Criteria In Solid Tumors (RECIST) 1.1 scan in October 2013, with noncomplete response-nonprogressive disease (in effect, SD) reported in the nontarget lesions (including brain metastases). The patient was ongoing with systemic PR as of May 1, 2015, 632 days after starting osimertinib.

Case study 2 is of a 59-year-old Asian female diagnosed with EGFRm (L858R) advanced NSCLC. This patient was previously treated with erlotinib between October 2011 and October 2012 (outcome: PR), pemetrexed/cisplatin/carboplatin for five cycles between October 2012 and January 2013 (SD), erlotinib between January 2013 and March 2013 (nonevaluable [NE]), docetaxel for three cycles between April 2013 and June 2013 (SD), and gemcitabine for two cycles between June 2013 and July 2013 (NE). Biopsy in August 2013 identified a T790M mutation. The patient started osimertinib 80 mg QD in a T790M positive expansion cohort of the AURA clinical study on September 2, 2013, and PR was achieved from the 6-week RECIST 1.1 scan in October 2013, with noncomplete response-nonprogressive disease (in effect, SD) reported in the nontarget lesions (including brain metastases). PR remained for the 12- and 18-week systemic assessments. Disease progression was observed in the brain as nontarget lesions at the 24-week scan in February 2014, although extracranial target lesions remained in response. The patient discontinued osimertinib on March 10, 2014, after 189 days on study treatment, and commenced vinorelbine on March 10, 2014, and whole brain irradiation on March 17, 2014.

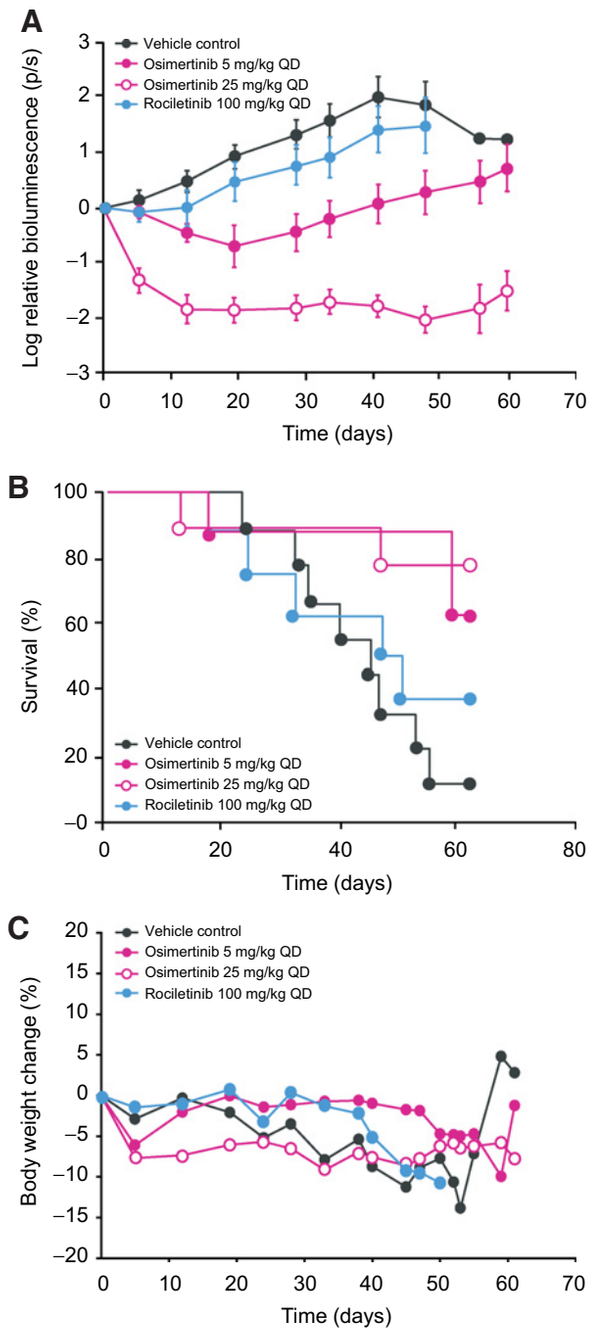

Figure 3.

Tumor bioluminescence (**A**), overall survival (**B**), and body weight (**C**) in a PC9 epidermal growth factor receptor exon 19 deletion mutation-positive mouse brain metastases model during treatment with osimertinib 5 and 25 mg/kg once daily (QD), rociletinib 100 mg/kg QD, or vehicle.

Discussion

Identification of brain metastases in patients with NSCLC has increased over recent decades; contributing factors include improved survival as a result of more effective systemic therapies, and improved imaging quality and accessibility allowing detection of asymptomatic lesions (36). Although approximately one-third of patients with NSCLC progress during treatment by the development of brain metastases (3), there are few effective treatment options available.

Traditionally, WBRT has been regarded as the cornerstone of treatment; however, there are concerns regarding its long-term neurotoxicity profile (37). In recent years, brain metastases management has been refined, and now includes local therapies such as surgical resection for single brain lesions and stereotactic radiosurgery for oligometastatic lesions (22).

Incomplete BBB penetration is widely viewed as the reason for the high prevalence of brain metastases in patients with NSCLC who have achieved good systemic control with chemotherapy regimens (20). As currently available EGFR-TKIs have a limited ability to penetrate the BBB, there remains an unmet need for EGFR-TKIs with improved clinical efficacy against brain lesions. This is particularly important as patients with EGFRm advanced NSCLC are living longer, and managing long-term neurotoxicity related to WBRT is challenging. We therefore describe preclinical

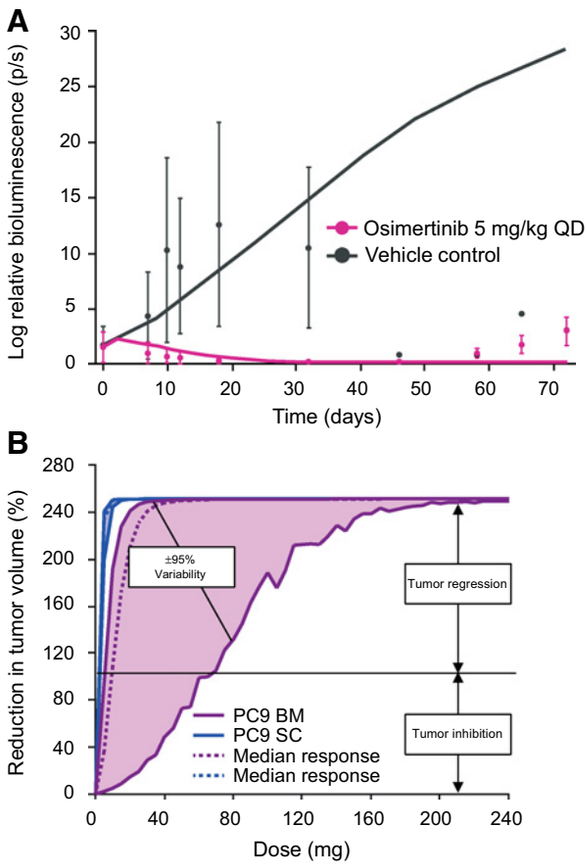

Figure 4.

Observed (marker) and predicted (solid lines) activity of osimertinib 5 mg/kg QD (once daily) in a PC9 brain metastases model in mice (**A**). Simulated osimertinib dose–response for brain metastases in patients using human pharmacokinetics, mouse brain penetration data, and the preclinical PKPD model (PC9 BM). The corresponding subcutaneous curves (PC9 SC) are shown for comparison. The two lines represent the 95% confidence interval of the dose–response (**B**).

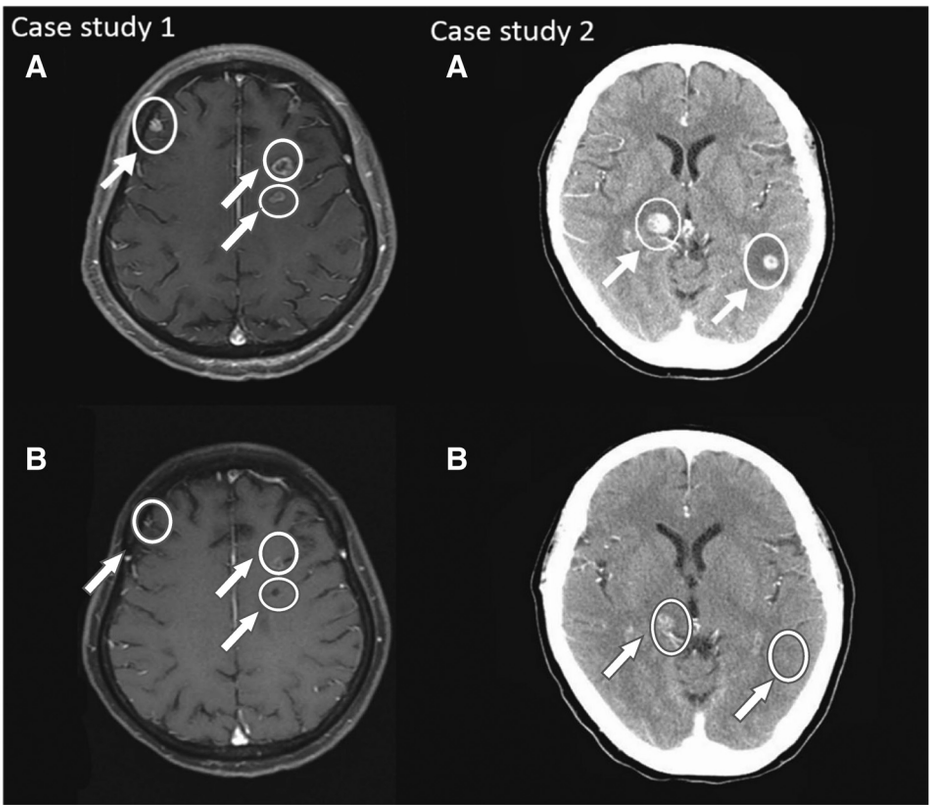

Figure 5.
Brain magnetic resonance imaging for case study 1 (**A**) baseline on July 23, 2013, and (**B**) July 2, 2014, and case study 2 (**A**) baseline on August 9, 2013, and (**B**) October 8, 2013.

and clinical evidence supporting that osimertinib may be an EGFR-TKI with improved brain exposure for treatment of brain metastases in the EGFRm NSCLC setting.

$Kp_{uu,brain}$ is well established as a good predictor of BBB permeability, with values greater than 0.3 indicative of good diffusion across the BBB (38). Osimertinib was shown to have a good $Kp_{uu,brain}$ value (0.39) compared with other currently available TKIs and rociletinib, suggesting it has the potential to achieve good brain exposure. This was despite evidence that osimertinib is a substrate of P-gp and BCRP efflux transporters, which are involved in the removal of toxins, drugs, and chemotherapies from the CNS, ultimately leading to drug resistance in the brain, when measured in cell lines (MDCK-MDR1, MDCK-BCRP) overexpressing these transporters (6–9). In the Caco2 cell line, which expresses P-gp/BCRP at physiological levels, osimertinib was the only agent without an efflux ratio, suggesting that permeability of osimertinib is sufficient to overcome the efflux in this nontransfected human cell line. In contrast, the other EGFR-TKIs assessed were restricted by efflux. By analogy, this same phenomenon could be happening at the BBB, resulting in the superior brain penetration of osimertinib, compared with the other TKI agents; however, these data need to be confirmed before any firm conclusions can be drawn. Kp_{uu} data presented here consistently showed that osimertinib could achieve significant exposure in the brain. Moreover, preclinical data showed that osimertinib caused durable shrinkage in an *in vivo* EGFRm brain metastases model at clinically relevant doses, consistent with its efficacy in extracranial preclinical models (25).

Importantly, the improved brain exposure of osimertinib indicated by these preclinical studies may result in improved clinical activity compared with currently available EGFR-TKIs, and also rociletinib. In these studies, osimertinib was more highly distributed to the mouse brain than gefitinib, afatinib, and rociletinib, and penetration of the rat brain was greater than previously described for gefitinib (39). Interestingly, low uptake into brain was also observed for erlotinib in xenografted mice (40). Osimertinib also demonstrated markedly more penetration of the nonhuman primate brain than rociletinib and gefitinib at microdosing levels. In the PC9 EGFRm mouse brain metastases model, osimertinib 25 mg/kg QD induced sustained tumor regression, with the antitumor activity correlating with overall survival. Although a dose of gefitinib 6.25 mg/kg, which roughly equates to a 250 mg QD human clinical dose, also demonstrated tumor regression, this was only for up to 20 days. Interestingly, consistent with distribution studies, no tumor regression was achieved with rociletinib at a dose of 100 mg/kg, and no survival benefit observed. It should be noted that at a dose of 25 mg/kg, plasma exposure of the active metabolites AZ5104 and AZ7550 was ~24% to 34% that of osimertinib, whereas human exposure of the metabolites has been reported as ~10% (41). In addition, the plasma terminal half-life of osimertinib was ~3 hours in mouse models, and reported as at least 50 hours in healthy volunteers (25).

An EGFR-TKI designed specifically to penetrate the BBB (AZD3759) is currently being investigated for treatment of patients with NSCLC with brain metastases. AZD3759 is active against EGFR-TKI sensitizing mutations, and preclinical evidence indicates that this compound shows good penetration of the BBB and induces profound tumor regression in animal models. In addition, in an ongoing phase I study in patients with EGFRm

NSCLC (BLOOM; NCT02228369), AZD3759 was well tolerated and was associated with intracranial tumor shrinkage (42). Although data are encouraging, it is important to note that, unlike osimertinib, this compound is not selective for T790M resistance mutations.

PET microdosing has been shown to be a robust method of predicting brain exposure compared with pharmacological dosing (43) and is comparable to microdialysis for confirming adequate brain exposure of CNS drug candidates (44). The low extent of brain exposure for gefitinib in the PET studies is consistent with human clinical experience, lending support to this approach being predictive. Indeed, PET microdosing in nonhuman primates has been used to confirm adequate brain exposure with AZD3241, a drug targeting the CNS to support to the conduct of phase IIa studies in patients (45, 46).

The greater distribution of osimertinib in the brain has the potential to translate into clinical benefit versus other EGFR-TKIs. Based on PKPD modeling, doses of up to 240 mg QD were simulated for brain metastases. These tumor growth simulations predicted that osimertinib at the current clinically recommended dose of 80 mg QD could be sufficient to target human EGFRm NSCLC brain metastases, although 160 mg QD may be more effective. This potency modeling is based on the observed lack of metabolite exposure in preclinical brain models, which contrasts to systemic plasma levels; it will be important to determine whether metabolites have similar lack of exposure in the clinical setting. Indeed, in strong support of these preclinical predictions, we also present early evidence of clinical activity of osimertinib in brain metastases, observed in two case studies of patients enrolled in the phase I AURA study. Both of these patients' cases achieved benefit from osimertinib treatment for controlling brain lesion growth.

The collective preclinical results reported here are promising, and suggest that osimertinib could offer a new clinically significant treatment option for patients with EGFRm brain metastases. Nonetheless, further investigation of osimertinib in patients with EGFRm NSCLC and brain metastases is warranted. An analysis of osimertinib PK in cerebrospinal fluid is an exploratory objective in the ongoing AURA3 (NCT02151981) trial, in which patients with EGFRm advanced NSCLC and stable brain metastases have been enrolled. As patients with brain metastases frequently present with concurrent leptomeningeal metastases (LM; ref. 47), osimertinib and AZD3759 are also being investigated in patients with LM in a phase I study (NCT02228369).

Disclosure of Potential Conflicts of Interest

P. Ballard, M. Cantarini, and P. Johnstrom have ownership interest (including patents) in AstraZeneca. J.C-H. Yang reports receiving speakers bureau honoraria from and is a consultant/advisory board member for AstraZeneca. P. Janne has ownership interest (including patents) in Gatekeeper Pharmaceuticals, is a consultant/advisory board member for ACEA Bioscience, Ariad, AstraZeneca, Boehringer Ingelheim, Chugai Pharmaceuticals, Merrimack Pharmaceuticals, Pfizer, and Roche/Genentech, reports receiving commercial research grants from Astellas Pharmaceuticals and AstraZeneca, and post-marketing royalties from Dana Farber Cancer Institute-owned intellectual property on EGFR mutations, which is licensed to Lab Corp. No potential conflicts of interest were disclosed by the other authors.

Authors' Contributions

Conception and design: P. Ballard, J.W.T. Yates, Z. Yang, D.-W. Kim, J.C.-H. Yang, M. Cantarini, P. Johnström, K.S. Thress, D. Cross

Development of methodology: J.C.-H. Yang, M. Box, P. Johnström, J. Malmquist

Acquisition of data (provided animals, acquired and managed patients, provided facilities, etc.): J.C.-H. Yang, M. Cantarini, A. Jordan, P. Johnström, J. Malmquist, P.A. Jänne

Analysis and interpretation of data (e.g., statistical analysis, biostatistics, computational analysis): P. Ballard, J.W.T. Yates, Z. Yang, D.-W. Kim, J.C.-H. Yang, M. Cantarini, K. Pickup, P. Johnström, K. Varnäs, K.S. Thress, D. Cross

Writing, review, and/or revision of the manuscript: P. Ballard, J.W.T. Yates, Z. Yang, D.-W. Kim, J.C.-H. Yang, M. Cantarini, K. Pickup, A. Jordan, M. Hickey, M. Grist, M. Box, P. Johnström, K. Varnäs, J. Malmquist, K.S. Thress, P.A. Jänne, D. Cross

Administrative, technical, or material support (i.e., reporting or organizing data, constructing databases): P. Ballard, M. Grist, J. Malmquist

Study supervision: P. Ballard, M. Cantarini, D. Cross

Other (synthesis of the chemical compounds for labeling and use in the studies): M. Box

Acknowledgments

We thank Jon Moran, PhD, from iMed Comms, an Ashfield Company, part of UDG healthcare plc, who provided medical writing support funded by AstraZeneca. We also thank Sue Ashton and Martine Mellor (plasma and brain *in vivo*), Ryan Bragg (radiolabels), and M. Raymond V. Finlay (coordination of chemistry) from AstraZeneca, members of the Karolinska Institutet PET group (PET micro-dosing), and Ziqiang Cheng and Kan Chen (ICC; gefitinib *in vitro* brain binding data) for their contributions to these studies.

Grant Support

This research was funded by AstraZeneca.

The costs of publication of this article were defrayed in part by the payment of page charges. This article must therefore be hereby marked *advertisement* in accordance with 18 U.S.C. Section 1734 solely to indicate this fact.

Received February 12, 2016; revised June 8, 2016; accepted July 5, 2016; published OnlineFirst July 19, 2016.

References

1. National Comprehensive Cancer Network. NCCN clinical practice guidelines in oncology NSCLC (version 7.2015), 2015 [cited 2015 Jul 16]. Available from: http://www.nccn.org/professionals/physician_gls/pdf/nscl.pdf.
2. Masters GA, Temin S, Azzoli CG, Giaccone G, Baker S Jr, Brahmer JR, et al. Systemic therapy for Stage IV non-small-cell lung cancer: American Society of Clinical Oncology Clinical Practice Guideline update. J Clin Oncol 2015;33:3488–515.
3. Mujoomdar A, Austin JH, Malhotra R, Powell CA, Pearson GD, Shiau MC, et al. Clinical predictors of metastatic disease to the brain from non-small cell lung carcinoma: primary tumor size, cell type, and lymph node metastases. Radiology 2007;242:882–8.
4. Heon S, Yeap BY, Britt GJ, Costa DB, Rabin MS, Jackman DM, et al. Development of central nervous system metastases in patients with advanced non-small cell lung cancer and somatic EGFR mutations treated with gefitinib or erlotinib. Clin Cancer Res 2010;16:5873–82.
5. Garg P, Dhakne R, Belekar V. Role of breast cancer resistance protein (BCRP) as active efflux transporter on blood-brain barrier (BBB) permeability. Mol Divers 2015;19:163–72.
6. Togashi Y, Masago K, Masuda S, Mizuno T, Fukudo M, Ikemi Y, et al. Cerebrospinal fluid concentration of gefitinib and erlotinib in patients with non-small cell lung cancer. Cancer Chemother Pharmacol 2012;70:399–405.

7. Bartolotti M, Franceschi E, Brandes AA. EGF receptor tyrosine kinase inhibitors in the treatment of brain metastases from non-small-cell lung cancer. Expert Rev Anticancer Ther 2012;12:1429–35.
8. Ding YL, Shih YH, Tsai FY, Leong MK. In silico prediction of inhibition of promiscuous breast cancer resistance protein (BCRP/ABCG2). PLoS One 2014;9:e90689.
9. Elmeliegy MA, Carcaboso AM, Tagen M, Bai F, Stewart CF. Role of ATP-binding cassette and solute carrier transporters in erlotinib CNS penetration and intracellular accumulation. Clin Cancer Res 2011;17:89–99.
10. Lampson LA. Monoclonal antibodies in neuro-oncology: getting past the blood-brain barrier. MAbs 2011;3:153–60.
11. Pardridge WM. Drug transport across the blood-brain barrier. J Cereb Blood Flow Metab 2012;32:1959–72.
12. Heon S, Yeap BY, Lindeman NI, Joshi VA, Butaney M, Britt GJ, et al. The impact of initial gefitinib or erlotinib versus chemotherapy on central nervous system progression in advanced non-small cell lung cancer with EGFR mutations. Clin Cancer Res 2012;18:4406–14.
13. Hoffknecht P, Tufman A, Wehler T, Pelzer T, Wiewrodt R, Schutz M, et al. Efficacy of the irreversible ErbB family blocker afatinib in epidermal growth factor receptor (EGFR) tyrosine kinase inhibitor (TKI)-pretreated non-small-cell lung cancer patients with brain metastases or leptomeningeal disease. J Thorac Oncol 2015;10:156–63.
14. Iuchi T, Shingyoji M, Sakaida T, Hatano K, Nagano O, Itakura M, et al. Phase II trial of gefitinib alone without radiation therapy for Japanese patients with brain metastases from EGFR-mutant lung adenocarcinoma. Lung Cancer 2013;82:282–7.
15. Park SJ, Kim HT, Lee DH, Kim KP, Kim SW, Suh C, et al. Efficacy of epidermal growth factor receptor tyrosine kinase inhibitors for brain metastasis in non-small cell lung cancer patients harboring either exon 19 or 21 mutation. Lung Cancer 2012;77:556–60.
16. Grommes C, Oxnard GR, Kris MG, Miller VA, Pao W, Holodny AI, et al. "Pulsatile" high-dose weekly erlotinib for CNS metastases from EGFR mutant non-small cell lung cancer. Neuro Oncol 2011;13:1364–9.
17. Committee for Medicinal Products for Human Use. Committee for Medicinal Products for Human Use (CHMP) assessment report for Giotrif (afatinib). European Medicines Agency 2013.
18. de Vries NA, Buckle T, Zhao J, Beijnen JH, Schellens JH, van Tellingen O. Restricted brain penetration of the tyrosine kinase inhibitor erlotinib due to the drug transporters P-gp and BCRP. Invest New Drugs 2012;30:443–9.
19. European Medicines Agency. Iressa summary of product characteristics, 2009[cited 2015 Oct 22].
20. Omuro AM, Kris MG, Miller VA, Franceschi E, Shah N, Milton DT, et al. High incidence of disease recurrence in the brain and leptomeninges in patients with nonsmall cell lung carcinoma after response to gefitinib. Cancer 2005;103:2344–8.
21. Fidler IJ, Yano S, Zhang RD, Fujimaki T, Bucana CD. The seed and soil hypothesis: vascularisation and brain metastases. Lancet Oncol 2002; 3:53–7.
22. Zimmermann S, Dziadziuszko R, Peters S. Indications and limitations of chemotherapy and targeted agents in non-small cell lung cancer brain metastases. Cancer Treat Rev 2014;40:716–22.
23. Rangachari D, Yamaguchi N, VanderLaan PA, Folch E, Mahadevan A, Floyd SR, et al. Brain metastases in patients with EGFR-mutated or ALK-rearranged non-small-cell lung cancers. Lung Cancer 2015;88:108–11.
24. Li J, Bentzen SM, Li J, Renschler M, Mehta MP. Relationship between neurocognitive function and quality of life after whole-brain radiotherapy in patients with brain metastasis. Int J Radiat Oncol Biol Phys 2008;71:64–70.
25. Cross DA, Ashton SE, Ghiorghiu S, Eberlein C, Nebhan CA, Spitzler PJ, et al. AZD9291, an irreversible EGFR TKI, overcomes T790M-mediated resistance to EGFR inhibitors in lung cancer. Cancer Discov 2014; 4:1046–61.
26. Finlay MR, Anderton M, Ashton S, Ballard P, Bethel PA, Box MR, et al. Discovery of a potent and selective EGFR inhibitor (AZD9291) of both sensitizing and T790M resistance mutations that spares the wild type form of the receptor. J Med Chem 2014;57:8249–67.
27. Sequist LV, Soria JC, Goldman JW, Wakelee HA, Gadgeel SM, Varga A, et al. Rociletinib in EGFR-mutated non-small-cell lung cancer. N Engl J Med 2015;372:1700–9.
28. U.S. Food and Drug Administration. FDA approves new pill to treat certain patients with non-small cell lung cancer, 2015 [cited 2015 Nov 13]. Available from:http://www.fda.gov/NewsEvents/Newsroom/PressAnnouncements/ucm472525.htm.
29. Varrone A, Sjöholm N, Eriksson L, Gulyas B, Halldin C, Farde L. Advancement in PET quantification using 3D-OP-OSEM point spread function reconstruction with the HRRT. Eur J Nucl Med Mol Imaging 2009;36: 1639–50.
30. Hochgrafe K, Mandelkow EM. Making the brain glow: in vivo bioluminescence imaging to study neurodegeneration. Mol Neurobiol 2013;47: 868–82.
31. Kemper EM, Leenders W, Kusters B, Lyons S, Buckle T, Heerschap A, et al. Development of luciferase tagged brain tumour models in mice for chemotherapy intervention studies. Eur J Cancer 2006;42:3294–303.
32. Schackert G, Fan D, Nayar R, Fidler IJ. Arrest and retention of multilamellar liposomes in the brain of normal mice or mice bearing experimental brain metastases. Sel Cancer Ther 1989;5:73–9.
33. Schackert G, Fidler IJ. Site-specific metastasis of mouse melanomas and a fibrosarcoma in the brain or meninges of syngeneic animals. Cancer Res 1988;48:3478–84.
34. Yates JW, Ashton S, Cross D, Mellor MJ, Powell SJ, Ballard P. Irreversible inhibition of EGFR: Modelling the combined Pharmacokinetic-Pharmacodynamic relationship of osimertinib and its active metabolite AZ5104. Mol Cancer Ther 2016; Jul 20. pii: molcanther.0142.2016. [Epub ahead of print]
35. Jänne PA, Yang JC, Kim DW, Planchard D, Ohe Y, Ramalingam SS, et al. AZD9291 in EGFR inhibitor-resistant non-small-cell lung cancer. N Engl J Med 2015;372:1689–99.
36. Norden AD, Wen PY, Kesari S. Brain metastases. Curr Opin Neurol 2005; 18:654–61.
37. McTyre E, Scott J, Chinnaiyan P. Whole brain radiotherapy for brain metastasis. Surg Neurol Int 2013;4:S236–44.
38. Varadharajan S, Winiwarter S, Carlsson L, Engkvist O, Anantha A, Kogej T, et al. Exploring in silico prediction of the unbound brain-to-plasma drug concentration ratio: model validation, renewal, and interpretation. J Pharm Sci 2015;104:1197–206.
39. McKillop D, Hutchison M, Partridge EA, Bushby N, Cooper CM, Clarkson-Jones JA, et al. Metabolic disposition of gefitinib, an epidermal growth factor receptor tyrosine kinase inhibitor, in rat, dog and man. Xenobiotica 2004;34:917–34.
40. Memon AA, Jakobsen S, Dagnaes-Hansen F, Sorensen BS, Keiding S, Nexo E. Positron emission tomography (PET) imaging with [11C]-labeled erlotinib: a micro-PET study on mice with lung tumor xenografts. Cancer Res 2009;69:873–8.
41. Planchard D, Dickinson PA, Brown KH, Kim D, Kim S, Ohe Y, et al. Preliminary AZD9291 Western and Asian clinical pharmacokinetics in patients and healthy volunteers: implications for formulation, dose and dosing frequency in pivotal clinical studies. Ann Oncol 2014;25(Suppl 4): Abstract 464P.
42. Kim D, Yang JC, Chen K, Cheng Z, Yin L, Martin PD, et al. AZD3759, an EGFR inhibitor with blood brain barrier (BBB) penetration for the treatment of non-small cell lung cancer (NSCLC) with brain metastasis (BM): preclinical evidence and clinical cases. J Clin Oncol 33, 2015 (suppl; abstr 8016).
43. Schou M, Varnäs K, Lundquist S, Nakao R, Amini N, Takano A, et al. Large variation in brain exposure of reference CNS drugs: a PET study in nonhuman primates. Int J Neuropsychopharmacol 2015;18:pii: pyv036.
44. Johnström P, Varnäs K, Bergman L, Malmquist J, Halldin C, Farde L. Estimation of the unbound brain to plasma ratio for CNS drug candidates—comparing results obtained with PET microdosing and microdialysis in non-human primates. J Labelled Compd Radiopharm 2015;58:S314.
45. Johnström P, Bergman L, Varnäs K, Malmquist J, Halldin C, Farde L. Development of rapid multistep carbon-11 radiosynthesis of the myeloperoxidase inhibitor AZD3241 to assess brain exposure by PET microdosing. Nucl Med Biol 2015;42:555–60.
46. Jucaite A, Svenningsson P, Rinne JO, Cselenyi Z, Varnäs K, Johnström P, et al. Effect of the myeloperoxidase inhibitor AZD3241 on microglia: a PET study in Parkinson's disease. Brain 2015;138:2687–700.
47. Herrlinger U, Forschler H, Kuker W, Meyermann R, Bamberg M, Dichgans J, et al. Leptomeningeal metastasis: survival and prognostic factors in 155 patients. J Neurol Sci 2004;223:167–78.